ISTITUTO NAZIONALE DI FISICA NUCLEARE
Laboratori Nazionali di Frascati

LNF-81/6(R)
28 Gennaio 1981

R. Boni, S. Guiducci and M. Vescovi: A NEW SYSTEM FOR POSITRON FOCUSING AT THE FRASCATI LINAC.

Servizio Documentazione
dei Laboratori Nazionali di Frascati
Cas. Postale 13 - Frascati (Roma)

INFN - Laboratori Nazionali di Frascati
Servizio Documentazione

LNF-81/6(R)
28 Gennaio 1981

R. Boni, S. Guiducci and M. Vescovi: A NEW SYSTEM FOR POSITRON FOCUSING AT THE FRASCATI LINAC.

1. - INTRODUCTION.

In the 350 MeV Frascati linear accelerator positrons are produced by a low energy (65 MeV) electron beam striking a copper target. Downstream from the target, positrons are focused by a short focal lenght magnetic lens and by eight long solenoids surrounding the accelerating sections.

The magnetic lens is used to match the emittance of the outcoming positrons (small dimensions and large divergence) to the acceptance of the Linac (large dimensions and small divergence). In order to achieve this matching, a very high field short lens is needed. The original 1.8 Tesla D.C. lens has been in operation until june 1980. A schematic view of the focusing system is shown in Fig. 1.

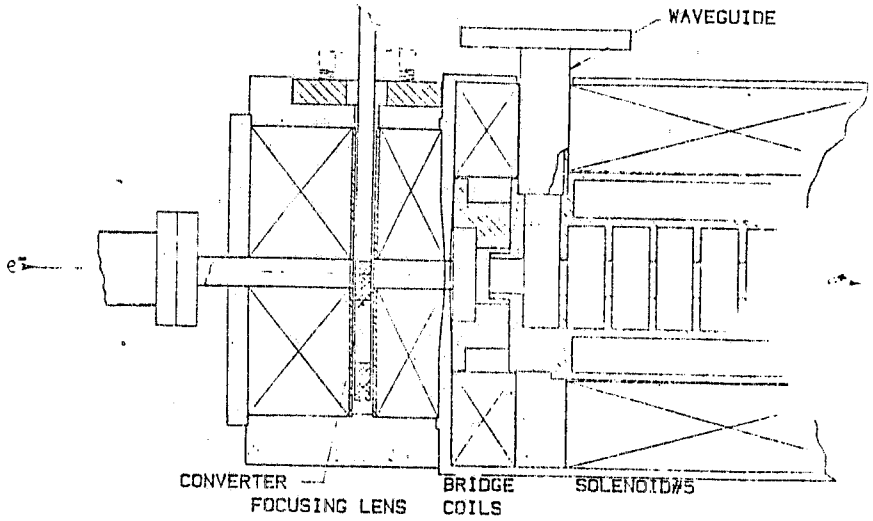

FIG. 1

Since the beam pulse lenght is 4 μs at a 200 Hz repetition rate the effective duty factor of such a D. C. lens was less than 10^{-3}.

The D. C. lens was placed outside the vacuum chamber and the converter was inside the lens, to have the positron source immersed in the uniform field region,which made the converter hard to get at for maintenance.

This matching section has now been replaced with a mechanically simpler new one, in which a small coil pulsed at 200 Hz maximum repetition rate is inserted[1]. A similar magnetic lens for positron focusing, working at 50 Hz, has been installed some time ago on Linac II at Desy[2] and a good capture efficiency has been obtained.

A Fortran program has been written, which calculates the acceptance of the matching lens and of the focusing system and the total positron current at the end of the Linac, in order to compare it with the calculations already done for the old lens[3, 4, 5]. The results of calculations and measurements performed on the system are presented.

2. - CHARACTERISTICS OF THE MATCHING LENS.

Fig. 2 shows the axial magnetic field B_z and the radial field B_r of the old lens together with the fringing field of the long solenoid N. 5 and of the bridge coils, which were used to maintain a uniform field in the region between the lens and the solenoid (Varian measurements[6]).

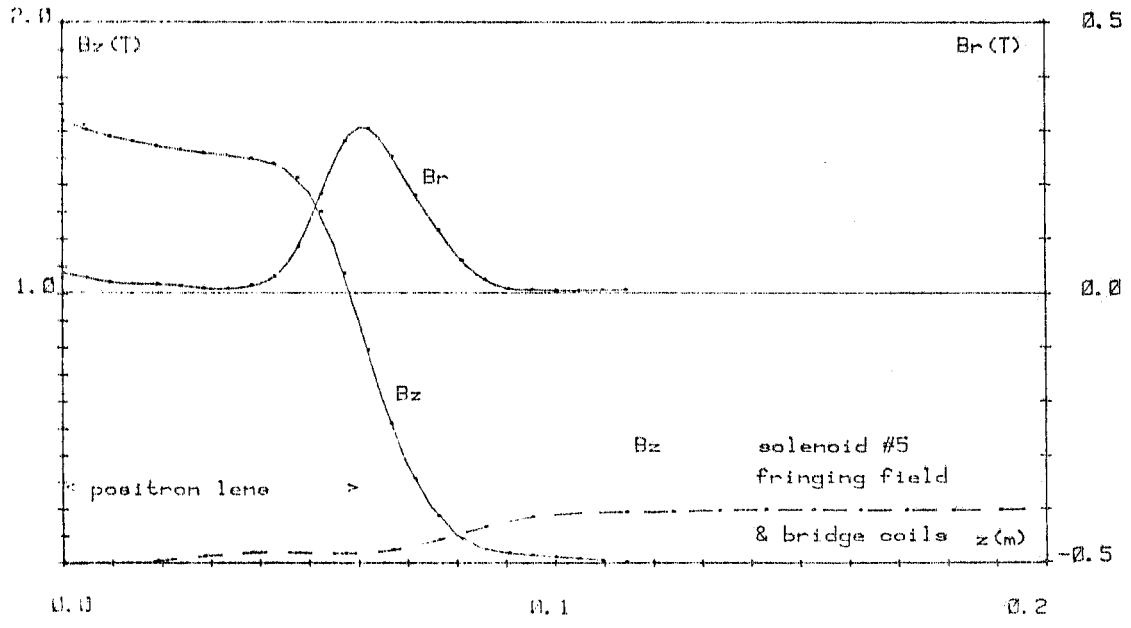

FIG. 2 - Old focusing system fields.

The new lens is a small copper coil and has been installed inside the vacuum chamber, just behind the converter (see Figs. 3 and 4). The magnetic field of the pulsed lens has been calculated from Biot-Savart's law integrating on the current distribution and neglecting empty spa-

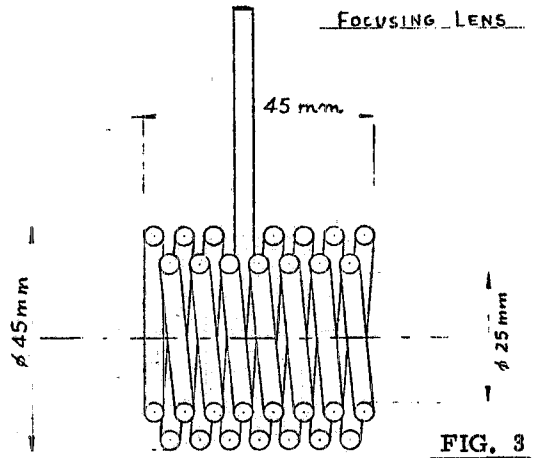

FIG. 3

ces between conductors[2].

The integrations have been performed numerically, using Simpson's method, and the integration step has been chosen to obtain a relative error of less than 1 %.

Fig. 5 shows the axial magnetic field B_z and the radial field B_r (r = 0.5 cm) along the axis for two coils with the following characteristics:

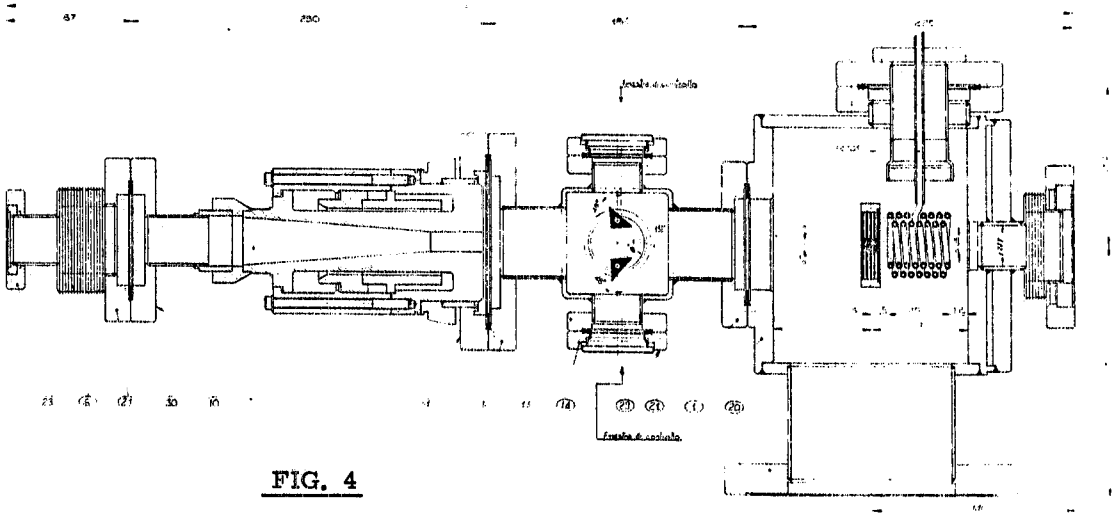

FIG. 4

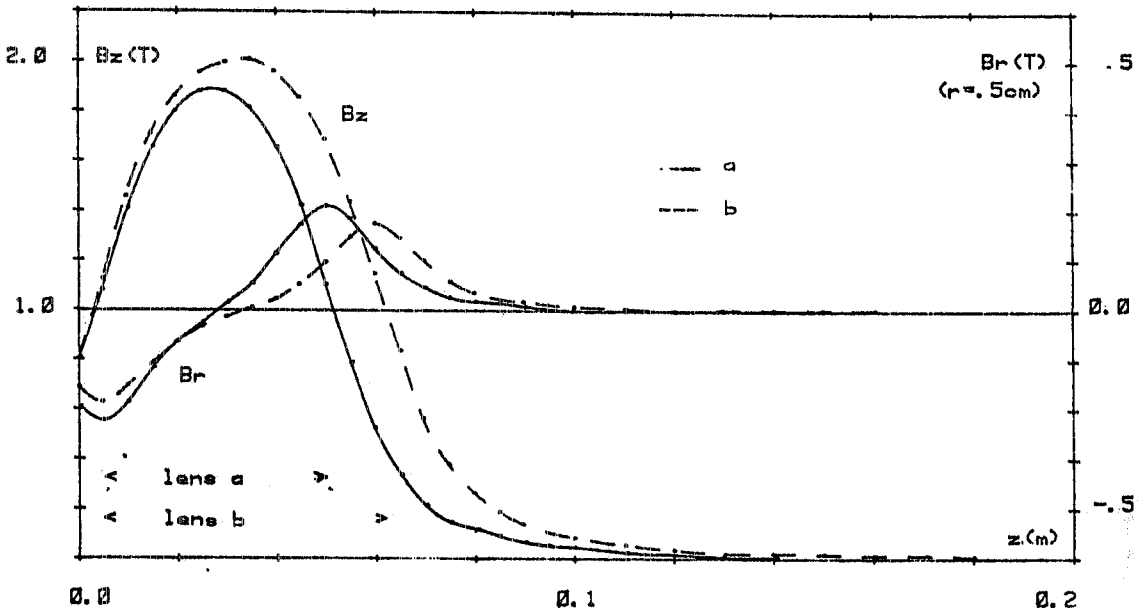

FIG. 5 - New focusing system fields.

	a) two layers of 8 turns each	b) two layers of 10 turns each
length	$L = 4.5$ cm	$L = 5.5$ cm
internal radius	$R_1 = 1.35$ cm	$R_1 = 1.35$ cm
external radius	$R_2 = 2.15$ cm	$R_2 = 2.15$ cm
current density	$J = 2.3778 \times 10^8$ Am^{-2}	$J = 2.3778 \times 10^8$ Am^{-2}

Fig. 4 represents only the region between the converter and the beginning of the first accelerating section; the distance between the coil and the converter is $\Delta z = 0.5$ cm. In this calculation we have neglected the effect of eddy currents induced on the converter, which is outside the lens, but immersed in its pulsed magnetic field. When the lens is powered at 40 KHz the skin depth for copper is 0.3 mm; therefore we assume that the magnetic field drops to zero 1 mm inside the converter. To give a rough estimate of this effect, we assume that the magnetic field remains unperturbed on the lens edge and vanishes in the region between the lens and the converter. The shape of the old lens magnetic field was almost rectangular and the axial field on the positron path was near its maximum all along the lens; the radial fringing field appeared only at the output edge.

The new lens has a bell shaped field like that of a short solenoid and is placed outside the converter. The positrons therefore see a lower average axial magnetic field, but cross the radial fringing field twice, once at the input and once at the output of the lens.

The calculations reported in the following show that the two lenses give nearly the same results as already demonstrated at DESY[2].

3. - POSITRON DISTRIBUTION AT THE CONVERTER.

The distribution of positrons coming out of the converter is not known with good accuracy; therefore we used approximate formulas from experimental measurements and values computed with Montecarlo methods[7].

Measurements made at Orsay and reported in Ref. (8) give the forward positron yield for an incident electron energy in the range $55\ \text{MeV} < E_- < 220\ \text{MeV}$; the converter material is lead and its thickness varies between $0.5\ X_0$ and $3\ X_0$ (X_0 = radiation lenght).

The yield does not change much with positron energy; for values of t around $1.5\ X_0$ it is roughly given by:

$$\frac{dN^+}{dE d\Omega} = N^- \, 2.4 \times 10^{-4} \, (E_{MeV} - 25)\ \text{MeV}^{-1}\ \text{sterad}^{-1} .$$

We assume a uniform energy distribution in the range $5\ \text{MeV} < E_+ < 15\ \text{MeV}$. For the radial and angular positron distribution we used the values from the Crawford and Messel[7] tables.

The values corresponding to an electron energy $E_- = 65$ MeV and a target thickness $t = 0.75\ X_0$ are obtained by linear interpolation and shown in Table I for a copper target and a lead target.

TABLE I

R/X_o	$E_- = 65$ MeV ; $t = 0.75\ X_o$	
	Copper	Lead
0.02	0.08	0.08
0.04	0.24	0.24
0.08	0.47	0.48
0.16	0.75	0.72
0.32	0.93	0.91
0.64	0.99	0.99
$\tilde{r}/X_o$	0.16	0.16

ϑ (rad)	$E_- = 65$ MeV ; $t = 0.75\ X_o$	
	Copper	Lead
0.02	0.005	0.003
0.04	0.02	0.01
0.08	0.06	0.06
0.16	0.20	0.21
0.32	0.49	0.52
0.64	0.82	0.85
1.28	1.00	0.99
$\tilde{\vartheta}$	0.49	0.49

The angular and radial distributions at $E_+ = 10$ MeV and $E_+ = 20$ MeV are almost the same, so that we assume they are independent of energy in the range considered. Table I shows that about 70 % of the positron beam is emitted inside a radius $\tilde{r}$ and an angle $\tilde{\vartheta}$, and ~95 % of the beam is inside $2\tilde{r}$ and $2\tilde{\vartheta}$. We have therefore assumed a gaussian distribution for r and ϑ with r.m.s. width $\tilde{r}$ and $\tilde{\vartheta}$.

Both for copper and for lead about 70 % of the positrons are emitted inside a radius $\tilde{r} = 0.16\ X_o$; therefore in order to minimize the source radius we should use a material with high density and small radiation lenght.

For copper	$D = 8.95\ g/cm^3$	$X_o = 1.45$ cm ,
For tungsten	$D = 19.1\ g/cm^3$	$X_o = 0.36$ cm ,
For gold	$D = 19.3\ g/cm^3$	$X_o = 0.34$ cm .

With a high density element like gold or tungsten the source radius is about a factor of four smaller than with copper.

4. - TRACKING PROGRAM.

The program "LEPOS" calculates the positron path from the converter to the input of the accelerating section N. 5 by integrating the motion equations step by step with the Runge-Kutta method[9]. The final positron current in a 1 % energy bin is calculated.

In cylindrical coordinates, the initial conditions of the particle are determined by the following variables :

E = energy ;

r = distance from the accelerator axis ;

z = coordinate along the accelerator axis ;

ϑ = angle between the particle momentum and the z axis ;

φ = azimuthal angle ;

α = angle between the transverse momentum of the particle and its radial component.

For each positron energy, random initial conditions are given with the following distribution function :

$$f(r, \vartheta, \alpha, E) = r\, e^{-r^2/(2\tilde{r}^2)}\, \vartheta\, e^{-\vartheta^2/(2\tilde{\vartheta}^2)}$$

in the range :

$$0 < \vartheta \lesssim 0.3 \text{ rad} ; \qquad 0 < r \lesssim 3 \text{ mm} ; \qquad 0 < \alpha \lesssim 2\pi .$$

The motion equations are solved step by step and for each step the condition $r < R_{max}$ is checked ; R_{max} (1 cm) is the free half aperture of the accelerating section. At the beginning of section N. 5 it is checked that the positron coordinates are accepted by the Linac focusing system, which is approximated by a continuous solenoid with uniform magnetic field (0.24 T) all along the Linac.

The final energy spread of the positron beam is calculated taking into account the phase spread of the electron bunch at the converter and the phase shift due to different paths of the positrons in the lens and in the solenoids. The formulas are given in Refs. (5) and (10).

The positron current has been calculated in two cases : pointlike and extended source. The width $\tilde{r}$ of the source is given by the combination of the width of the incident beam and the width due to multiple scattering in the target ; we have assumed $\tilde{r} = 1$ mm.

For pointlike source the maximum accepted angle at the converter is calculated and then the accepted solid angle Ω_{PS} is :

$$\Omega_{PS} = 2\pi \int_0^{\vartheta_{max}} e^{-\vartheta^2/(2\tilde{\vartheta}^2)} \sin\vartheta \, d\vartheta \cong 2\pi \int_0^{\vartheta_{max}} e^{-\vartheta^2/(2\tilde{\vartheta}^2)}\, \vartheta \, d\vartheta =$$

$$= 2\pi\, \vartheta^2 (1 - e^{-\vartheta^2_{max}/(2\tilde{\vartheta}^2)}) .$$

As ϑ_{max} is quite small, we use the approximation $\sin\vartheta \sim \vartheta$.

For the extended source we define an accepted solid angle Ω_{ES} as the mean value of the production solid angle of positrons accepted at the end of the accelerating structure.

The accepted solid angle $\Omega(E)$ has a maximum for an energy E_o and drops to zero in an interval ΔE.

In order to obtain the total acceptance we calculate $\Omega(E_i)$ for a set of energies E_i in the interval ΔE and add all Ω's up. The final positron current is :

$$i_+ = i_- \frac{1}{N^-} \frac{dN^+}{dE d\Omega} (\Sigma_i\, \Omega(E_i)\, \Delta E_i) =$$

$$= i_- 2.4 \times 10^{-4} (E_{MeV} - 25) (\Sigma_i\, \Omega(E_i)\, \Delta E_{i_{MeV}}) .$$

5. - RESULTS.

The expected positron current has been calculated for the following configurations of the focusing system:

a) D. C. magnetic lens described in par. 2. The magnetic field is shown in Fig. 2. The converter is inside the lens.

b) Pulsed magnetic lens as described in par. 2. The magnetic field is shown in Fig. 5a. The distance between lens and converter is Δ_z = 0.5 cm, and the effect of eddy currents is taken into account.

c) and d) Pulsed lens described in b); only the length is changed to L_c = 5.5 cm and L_d = 6.5 cm.

e) Same configuration as c); but eddy currents effect is neglected.

f) Same configuration as c). The distance between lens and converter is varied from 0.5 cm to 1 cm.

g) Same configuration as c). The maximum magnetic field is increased by 30%.

h) Same configuration as c). Bridge coils off and solenoid N. 5 fringing neglected.

The characteristics of the focusing system in the various cases are summarized in Table II; the computed accepted solid angles are reported in Table III.

TABLE II

	B_{max} (T)	N	I (KA)	L (cm)	R_1 (cm)	R_2 (cm)	Δz (cm)
a)	1.77	-----	0.546	6.2	---	---	---
b)	1.77	2 x 8	5.02	4.5	1.35	2.15	0.5
c)	1.77	2 x 10	4.59	5.5	1.35	2.15	0.5
d)	1.77	2 x 12	4.34	6.5	1.35	2.15	0.5
e)[1]	1.77	2 x 10	4.59	5.5	1.35	2.15	0.5
f)	1.77	2 x 10	4.59	5.5	1.35	2.15	1.0
g)	2.25	2 x 10	5.83	5.5	1.35	2.15	0.5
h)[2]	1.77	2 x 10	4.59	5.5	1.35	2.15	0.5

[1] Eddy currents in the converter have been neglected.
[2] The field of the bridge coils is zero and the solenoid N. 5 fringing field is neglected.

The values of ϑ_{max} and of the accepted solid angle Ω_{PS} for pointlike source as functions of energy are listed in the first two columns of Table III. The third and fourth columns show the value of the accepted solid angle for an extended source ($\tilde{r}$ = 1 mm); in the first case the values are calculated neglecting the final energy spread and in the second requiring a relative energy spread of less than 1%. The values of Table III are plotted in Fig. 6 for configura-

TABLE III

	E (MeV)	ϑ_{max} (rad)	$\Omega_{P.S.}$ (sterad)	$\Omega_{E.S.}$ (sterad)	$\Omega_{E.S.}$ (sterad) $\Delta E/E_f < 1\%$
a)	8	0.127	0.049	0.045	0.008
	8.5	0.164	0.080	0.072	0.045
	9	0.205	0.121	0.092	0.060
	9.5	0.253	0.177	0.114	0.075
	10	0.251	0.174	0.114	0.090
	10.5	0.184	0.100	0.078	0.057
	11	0.132	0.053	0.052	0.036
	11.5	0.105	0.034	0.032	0.021
b)	6	0.090	0.025	0.033	0.014
	6.5	0.122	0.045	0.069	0.045
	7	0.154	0.071	0.057	0.045
	7.5	0.208	0.124	0.092	0.080
	8	0.264	0.190	0.127	0.111
	8.5	0.298	0.233	0.151	0.134
	9	0.212	0.129	0.082	0.071
	9.5	0.139	0.058	0.057	0.029
c)	7.5	0.099	0.030	0.029	0.007
	8	0.120	0.044	0.040	0.025
	8.5	0.154	0.071	0.063	0.048
	9	0.196	0.112	0.092	0.080
	9.5	0.239	0.160	0.144	0.115
	10	0.246	0.168	0.118	0.109
	10.5	0.184	0.100	0.069	0.069
	11	0.133	0.054	0.031	0.019
d)	9.5	0.110	0.037	0.042	0.021
	10	0.132	0.053	0.040	0.031
	10.5	0.165	0.081	0.075	0.059
	11	0.196	0.112	0.099	0.091
	11.5	0.219	0.137	0.092	0.086
	12	0.196	0.112	0.071	0.069
	12.5	0.130	0.051	0.071	0.063
	13	0.112	0.038	0.040	0.018

	E (MeV)	ϑ_{max} (rad)	$\Omega_{P.S.}$ (sterad)	$\Omega_{E.S.}$ (sterad)	$\Omega_{E.S.}$ (sterad) $\Delta E/E_f < 1\%$
e)	8.5	0.131	0.052	0.045	0.025
	9	0.166	0.081	0.087	0.059
	9.5	0.205	0.121	0.111	0.084
	10	0.242	0.163	0.120	0.096
	10.5	0.232	0.152	0.082	0.078
	11	0.158	0.075	0.048	0.046
	11.5	0.120	0.044	0.052	0.045
	12	0.095	0.028	0.023	0.010
f)	8.5	0.109	0.036	0.021	0.011
	9	0.131	0.052	0.048	0.032
	9.5	0.166	0.081	0.063	0.052
	10	0.202	0.118	0.099	0.092
	10.5	0.230	0.149	0.137	0.126
	11	0.212	0.129	0.120	0.118
	11.5	0.148	0.066	0.045	0.038
	12	0.113	0.039	0.042	0.016
g)	10.5	0.127	0.049	0.052	0.032
	11	0.155	0.072	0.059	0.043
	11.5	0.180	0.095	0.085	0.072
	12	0.231	0.150	0.101	0.090
	12.5	0.242	0.163	0.106	0.097
	13	0.184	0.100	0.075	0.074
	13.5	0.142	0.060	0.052	0.045
	14	0.099	0.030	0.019	0.008
h)	7	0.062	0.012	0.019	0.013
	7.5	0.100	0.031	0.038	0.026
	8	0.137	0.057	0.035	0.029
	8.5	0.194	0.109	0.078	0.069
	9	0.243	0.164	0.104	0.092
	9.5	0.250	0.173	0.118	0.115
	10	0.157	0.074	0.073	0.054
	10.5	0.108	0.035	0.045	0.017

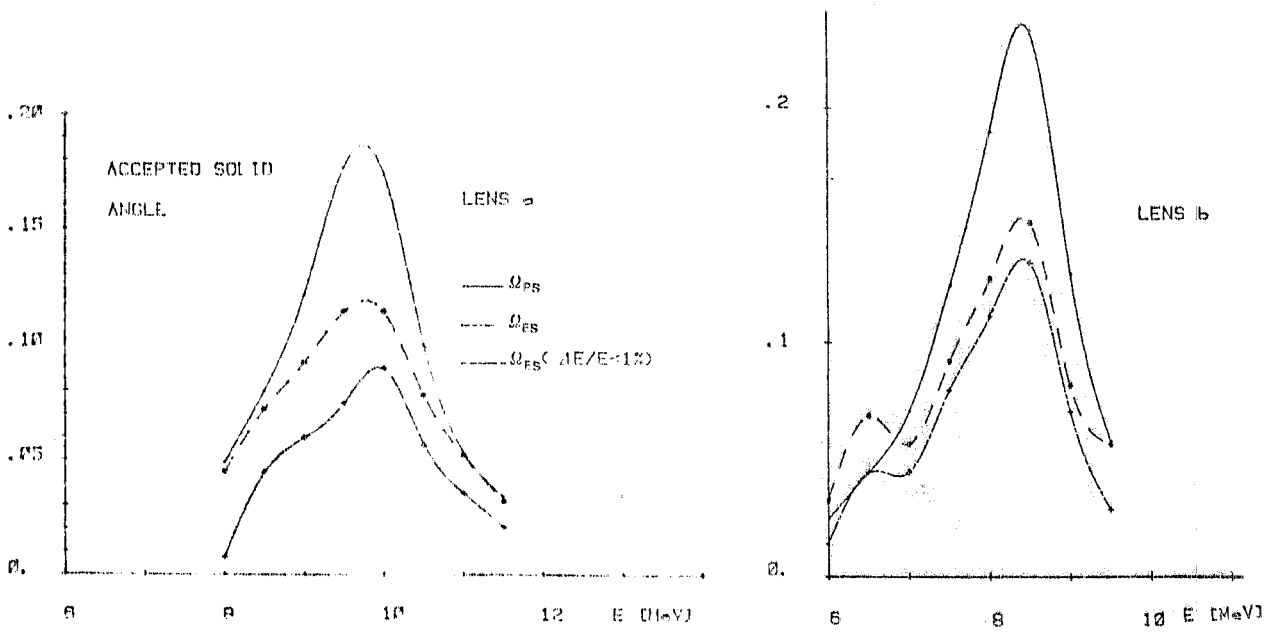

FIG. 6

tions a) and b), and in Figs. 7 and 8 for configurations b), c) and d).

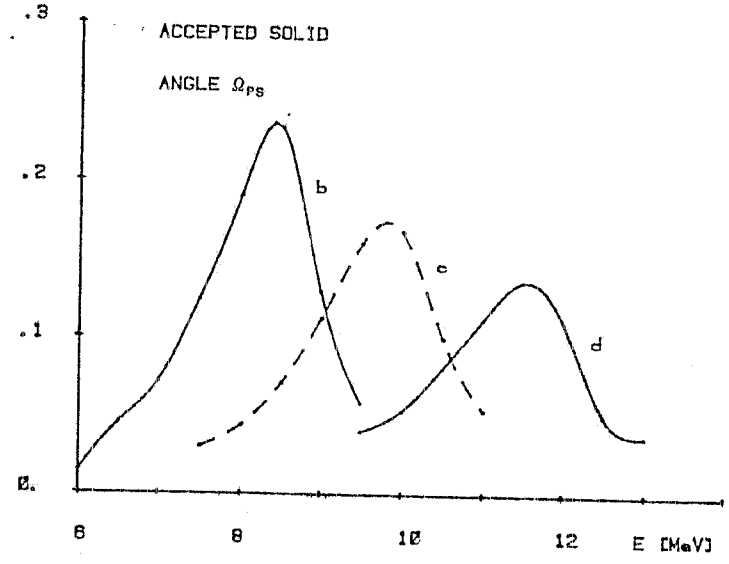

FIG. 7

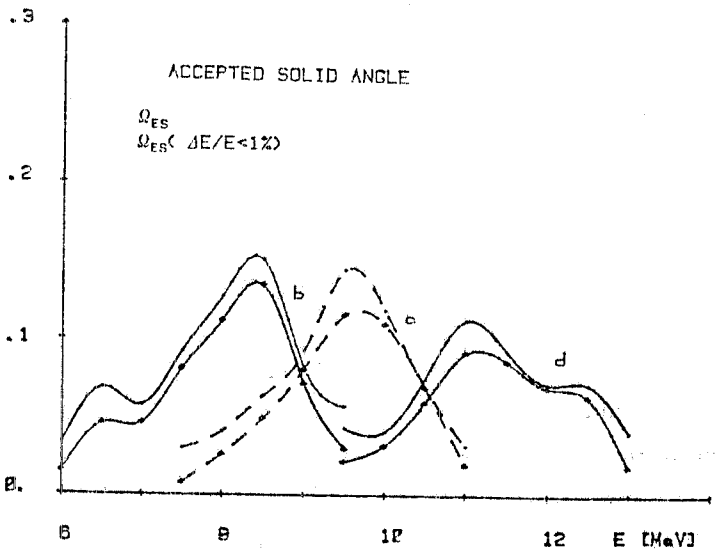

FIG. 8

The total acceptance of the system is calculated from the values of Table III as : $\Sigma_i \Omega(E_i) \Delta E_i$ and the final current is then obtained.

The results are given in Table IV ; in the first column the value E_o of the energy corresponding to the maximum accepted solid angle Ω ; in the second column the energy interval for which Ω is greater than 0.025 sterad ; in the third and fourth column the final positron current for pointlike source and for extended source respectively ; in the fifth column the final positron current in a 1% energy bin. As it can be seen from Table IV, if we require a final positron energy spread of less than 1%, the final positron current is not very sensitive to the lens parameters.

TABLE IV

	E_o (MeV)	ΔE (MeV)	I_{PS} (mA)	I_{ES} (mA)	I_{ES} $\Delta E/E < 1\%$ (mA)
a)	9.5	3.6	1.6	1.2	0.8
b)	8.5	3.7	1.8	1.3	1.1
c)	10.0	3.2	1.5	1.2	0.9
d)	11.5	3.5	1.2	1.1	0.9
e)	10.0	3.6	1.4	1.1	0.9
f)	10.5	3.2	1.3	1.2	1.0
g)	12.5	3.5	1.4	1.1	0.9
h)	9.5	3.3	1.3	1.0	0.8

In fact if the angular acceptance of the lens increases, the phase shift due to different paths in the lens increases too and so does the final energy spread. Moreover the positron distribution at the converter is nearly uniform in ϱ, ϑ and E in the range of interest; therefore a variation in the focusing system parameters changes the set of ϱ, ϑ and E corresponding to the maximum acceptance, but does not appreciably modify the final positron current.

The results of Table IV illustrate how different parameters affect the final current.

We want to compare the efficiency of the old D. C. lens (item a)) with the new pulsed one (item b)). From Table IV and Fig. 6 we see that the pulsed lens gives a final current ~10% greater than the D. C. lens (see also Ref. (2)), if we do not consider the final energy spread; moreover if we require a final energy spread smaller than 1%, the fraction of current within this interval is larger for the pulsed lens.

The difference between the two lenses is mainly due to their different lenght: the focal plane of the new lens is nearer to the converter giving a larger angular acceptance. In fact the lens of item c), which is similar to lens b), but 1 cm longer, gives nearly the same results as the old D. C. lens. The dependence on the length of the lens is shown in Figs. 7 and 8 where three lenses of different lengths are compared.

The effect of eddy currents in the converter is not significant, as it can be seen by comparing c) and e).

If we vary the distance between lens and converter from 0.5 cm to 1 cm (see c) and f)) the current for pointlike source decreases, but for an extended source it is nearly the same. If we increase the magnetic field of the lens (see c) and g)) the acceptance does not change, but the energy E_o increases linearly with magnetic field; as we consider an uniform energy distribution of the positrons, this does not affect the final current.

Comparing c) and h) we can see that the fringing field of solenoid N. 5 and the field of the bridge coils raises the total current I_{ES} by ~10%. From this calculation lens b) appears to be the best choice; within our approximations it gives the maximum positron current.

For technical reasons it is not worthwhile to try and get a better acceptance by further decreasing the length of the lens, while keeping the same field integral.

A way to increase the positron current is to reduce the source radius by optimizing the focusing of incident electrons on the converter, or using a converter with a smaller radiation length.

The lens which has finally been installed on the Linac (see Fig. 3) is similar to lens b), but has 15 turns instead of 16, so its maximum field is slightly smaller and will capture lower energy positrons. This might give a slightly lower efficiency due to the lower positron yield for energies $E_- < 5$ MeV.

6. - THE PULSE GENERATOR.

The focusing lens is powered by a pulse generator located outside the Linac tunnel for case of maintenance and the connection to the lens is made via twenty 30 Ω coaxial cables in parallel to keep the inductance of the link low.

A simplified diagram of the pulse generator is shown in Fig. 9 while the complete circuit diagram is shown in Fig. 10.

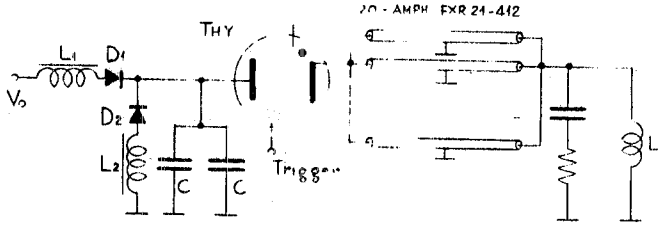

FIG. 9

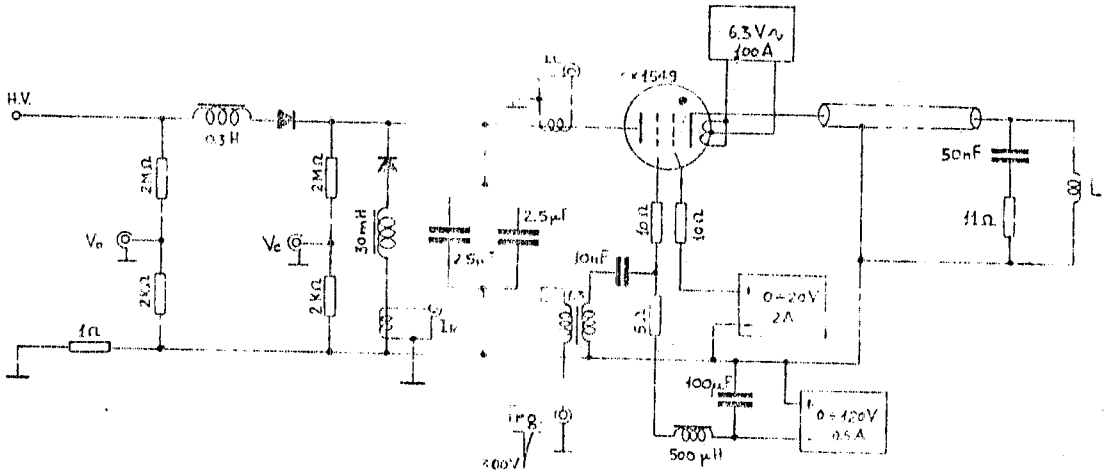

FIG. 10 PULSE GENERATOR -

The discharge of the capacitors C through the lens L produces the required magnetic field pulse. The switching element is an EEV CX 1549 Deuterium filled thyratron, synchronized with the Linac beam pulses. The series L_2D_2 allows the recovery of part of the energy stored in the capacitors, so that the supply has to provide only the power dissipated by Joule effect.

Apart from resistive, the charging voltage of C is twice the supply voltage.

The inductance L_T of the lens (the lens is shown in Fig. 3) plus the connection cables is $\approx 3.5\ \mu H$.

With:

$$2C = 5\ \mu F \qquad \text{and} \qquad V_C = 4\ kV\ ,$$

the peak current in the lens is:

$$I_p = \frac{V_C}{\omega L_T}\, e^{-(RT/8L_T)} = 4400\ A\ ,$$

where:

$R = 0.11$ Ohmic losses in the pulse forming network;

$\omega = \sqrt{\frac{1}{2L_TC} - \frac{R^2}{4L_T^2}} = 2.38 \times 10^5$ rad/sec damped angular frequency;

$T/2 = 13\ \mu sec$ pulse length.

The capacitor voltage and the lens current during the discharge time are shown in Fig. 11 (not to scale).

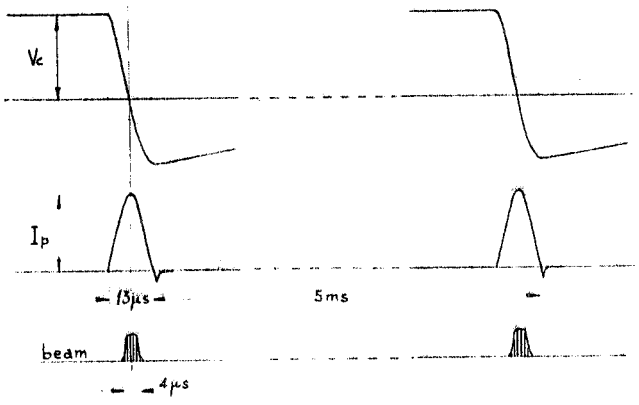

FIG. 11

A typical set of operation parameters is:

Supply voltage	V_o	= 2.2 kV
Charging voltage	V_C	= 4 kV
Peak current	I_p	= 4.4 kA
Peak magnetic field	B_p	= 15 kG
Repetition rate	f_{max}	= 200 p.p.s.

Pulse length	τ	= 13 μsec
Charging inductance	L_1	= 0.3 H
Recovery inductance	L_2	= 30 mH
Lens inductance	L	= 3.3 μH
Energy storage capacitor	C	= 2.5 μF/15 kV
Average Ohmic losses	W_a	= 3 kW.

The capacitors are water cooled and chokes L_1, L_2 are immersed in oil. The power dissipation in the focusing coil, constructed from a copper tube, is 300 W at 200 Hz. The coil is water cooled (distillated water).

Fig. 4 shows a top view of the converter and positron focusing equipment installed on the Linear Accelerator. The vacuum tank containing the lens and the target can be seen on the right hand side of the drawing. A system is provided (center of drawing) to monitor the beam-spot on the target.

The assembled pulse generator is shown in Fig. 12. The system has now been in operation for over six months without problems.

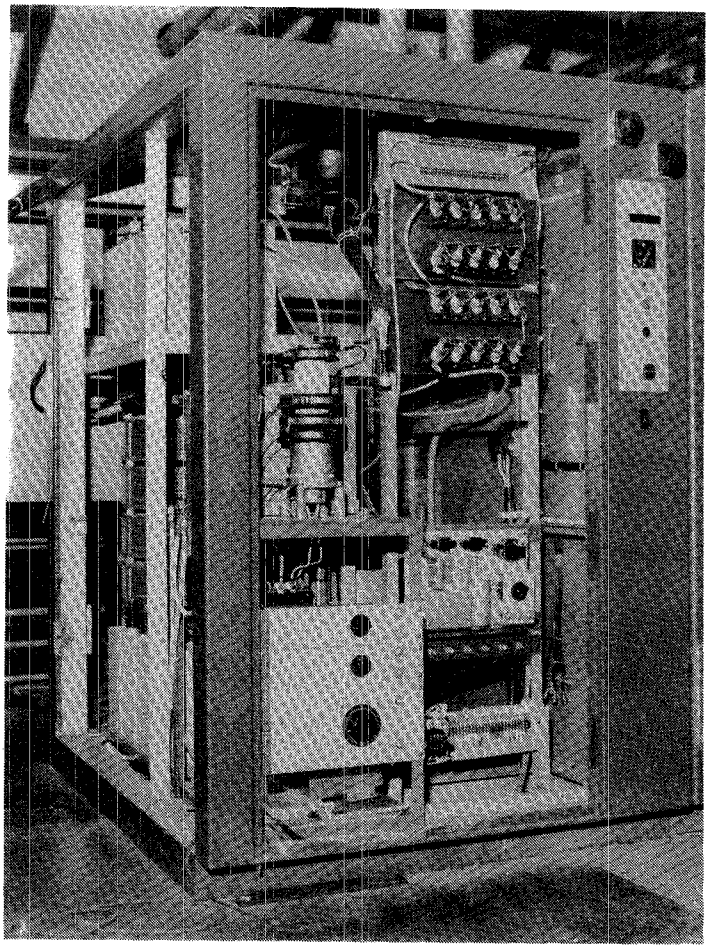

FIG. 12

ACKNOWLEDGEMENTS.

We wish to thank the LNF Technical Division for designing and constructing the vacuum vessel. The help of the Linac Staff, and especially of Mr. Pella and Mr. Simeoni, who assembled the pulse generator, and their precious assistance during the tests are also gratefully acknowledged.

REFERENCES.

(1) - R. Boni e M. Vescovi, Adone Internal Memo L-46 (1979); L-53 (1980).

(2) - G. Stange, A pulsed magnetic lens for positron focusing. Numerical calculations and first measurements with a prototype, Report DESY S1-73/4 (1973).

(3) - F. Amman, Positron accelerators, in 'Linear Accelerators', ed. by P. Lapostolle and A. L. Septier (North-Holland, 1970).

(4) - E. Ferlenghi e L. Mango, Calcoli per l'ottica di trasporto dei positroni nell'acceleratore lineare di Frascati, Frascati Report LNF-63/70 (1963).

(5) - E. Ferlenghi e L. Mango, Calcoli per l'ottica di trasporto nel Linac di Frascati di positroni accelerati da un'onda non piana, Frascati Report LNF-64/5 (1964).

(6) - VARIAN 'Frascati positron converter system' (April, 1965).

(7) - H. Messel and D. F. Crawford, Electron-photon Shower Distribution Function Tables for Lead, Copper and Air Absorbers (Pergamon Press, 1970).

(8) - J. Haissinski, Focusing devices for a positron beam at the linear accelerator of Orsay, Nuclear Instr. and Meth. 51, 181 (1967).

(9) - W. Gear, Numerical initial Value Problems in Ordinary Differential Equations (Prentice Hall, 1971).

(10) - F. Amman e R. Andreani, L'acceleratore lineare per elettroni e positroni, Frascati Report LNF-63/46 (1963).